# Single Heartbeat Cardiac Tagging for the Evaluation of Transient Phenomena

Daniel A. Herzka,[1,2,3]* J. Andrew Derbyshire,[2,3] Peter Kellman,[2] and Elliot R. McVeigh[1,2]

**Many cardiac abnormalities are of a transient nature, creating a beat-to-beat variation in myocardial function. This work presents the cardiac imaging technique for the measurement of regional function during transient cardiac phenomena. All information necessary for the reconstruction of a cine loop is acquired within a single heartbeat, avoiding the temporal blurring introduced by segmented imaging due to the assumption of cardiac cycle periodicity. This method incorporates a gradient-optimized, high-efficiency EPI-SSFP sequence and TSENSE parallel imaging. For acquisitions with readout resolutions of 128,160, 192, and 256 points, the technique produced images with average temporal resolution of 35, 39, 43, and 52 ms and average spatial resolutions of 2.65, 2.12, 1.77, and 1.32 mm in the readout direction, respectively, and 2.88 and 2.08 mm in the phase encode direction for acceleration rates of 3 and 4, respectively. Local apparent strains in the single slice and measurements of ventricular end-systolic and end-diastolic areas were used as quantitative measures to validate the single heartbeat technique. To demonstrate the utility of the sequence, movie loops were acquired for multiple heartbeats in non-breath-held acquisitions as well as during a Valsalva maneuver. A heartbeat-interleaved acquisition allowed for the reconstruction of nonaccelerated images from *R* contiguous heartbeats. Images reconstructed from such data displayed tag blurring and reduced tag persistence due to motion and interheartbeat variability. Images acquired during the Valsalva maneuver demonstrated apparent beat-to-beat variability, visible both in the images and as changing strain patterns and ventricular volumes. Magn Reson Med 54:1455–1464, 2005. Published 2005 Wiley-Liss, Inc.†**

**Key words: myocardial tagging; myocardial function; fast cardiac imaging; parallel imaging; real time imaging; Valsalva maneuver**

Many myocardial abnormalities are transient in nature, leading to beat-to-beat variation in cardiac function. Generally, quantitative regional function is assessed using segmented *k*-space imaging, which acquires multiple cardiac phases over several heartbeats and assumes the periodicity of the cardiac cycle. *k*-space is partitioned into several segments, each of which is acquired repeatedly in separate heartbeats, and a given cardiac phase is reconstructed from the corresponding segments from each of the heartbeats. While this method reduces the temporal window of each image, typically referred to as the temporal resolution, it ignores the inherent averaging from the use of data obtained over multiple cardiac cycles and precludes the accurate imaging of transient phenomena that span multiple heartbeats. The presented technique acquires a complete cine loop of one slice position within a single heartbeat yielding a self-contained dataset that does not require the assumption of cardiac periodicity as it does not require temporal averaging. This technique opens new opportunities to investigate transitory changes in cardiac function such as respiratory effects on the heart, albeit without addressing issues of through-plane motion.

Real-time single heartbeat acquisitions have been presented before, even as early as 1987 by Chapman et al. (1). The necessary temporal and spatial resolution required to correctly assess cardiac function have also been described. Setser et al. (2) proposed that accurate measurement of left ventricular (LV) volume and ejection fraction requires sampling at 20–25 Hz or better (~40 ms temporal resolution) and 2 × 2 mm spatial resolution or better for resting heart rates and that better temporal resolutions are necessary for higher heart rates, such as seen during stress tests. These results imply that previous real-time works have lacked sufficient spatial and/or temporal resolution (3–8) necessary for clinically relevant measurements of transient events. For example, Schalla et al., Nagel et al., and Bornsted et al. (3–5) rely on the high efficiency achievable with echo-planar (EPI) techniques with nine readouts to achieve a spatial resolution of 2.2 × 4.4 mm (reduced spatial resolution) and were limited to a temporal resolution of 62 ms (i.e., 16-Hz sampling). Unfortunately, the use of EPI with long echotrain lengths (compared to the $T_2$* of the heart) leads to artifacts from off-resonance, motion and flow, and phase discontinuities that can have deleterious effects on image quality (9–12). Other work has relied upon the combined efficiency and signal-to-noise ratio (SNR) of TrueFISP or steady-state free precession (SSFP) for real-time applications (13,14). Lee et al. (6) used Cartesian sampling (55 ms and 2.7 × 4.2 mm) while Shankaranarayanan et al. (7), Schaeffter et al. (15), and Spuentrup et al. (16) use radial sampling (91, 80, and 100 ms and 2.5 (2), 2.3 (2), and 2.5 (2) mm, respectively) to achieve adequate temporal or spatial resolutions, but not both. Furthermore, all these works rely on view or echo sharing reconstructions, which reduce their true temporal resolution by a factor of 2 (17). Similarly, Nayak and Hu (8) have used very efficient spiral sampling to achieve nominal spatial resolutions of 1.88 × 1.88 mm at the cost of temporal resolution, 96 ms. Other studies have applied accelerated imaging to improve temporal resolution (18–20),

[1]Department of Biomedical Engineering, Johns Hopkins University School of Medicine Baltimore, Maryland, USA.

[2]Laboratory of Cardiac Energetics National Institutes of Health National Heart, Lung and Blood Institute, Bethesda, Maryland, USA.

[3]D. A. Herzka and J. A. Derbyshire contributed equally to this work.

*Correspondence to: Daniel A. Herzka, Laboratory of Cardiac Energetics, National Institutes of Health National Heart, Lung, and Blood Institute, 10 Center Drive, MSC-1061 Building 10, B1D416, Bethesda, MD 20892-1061, USA. E-mail: herzkad@nih.gov

Received 10 March 2004; revised 4 August 2005; accepted 12 August 2005.
DOI 10.1002/mrm.20719
Published online 1 November 2005 in Wiley InterScience (www.interscience.wiley.com).

but these studies have typically focused on low latency reconstructions and therefore lower acceleration rates, sacrificing potential gains in resolution. Although current real-time acquisitions have been shown to be accurate in reporting left ventricular function in the form of ejection fraction and myocardial wall volumes (2,4), the spatial and/or temporal resolution obtained may not be enough to detect regional variations in cardiac function.

This work presents the use of an ECG-triggered, fast and efficient imaging technique combined with high acceleration parallel imaging that provides high spatial and temporal resolution images without view sharing ideal for imaging transient wall motion patterns from individual cardiac cycles. The data acquisition methods are similar to those used in so-called real-time imaging techniques. However, we avoid the specific use of the term "real-time" here because it suggests low latency reconstruction, which, although possible, was not implemented in the current work. The method incorporates the use of hardware optimized gradient waveforms (21,22) combined with a high efficiency three-echo EPI-SSFP sequence (23) and an adaptive parallel imaging technique, TSENSE (adaptive sensitivity encoding incorporating temporal filtering) (24). Finally, myocardial tagging (25–27) is used to provide a measure of regional cardiac function. All combined, this technique provides images with an unprecedented combination of spatial and temporal resolution (i.e., 1.7 × 2.0 mm, 43 ms) for the measurement of changes within a single slice through the heart within a single heartbeat and the investigation of phenomena that exhibit beat-to-beat variation.

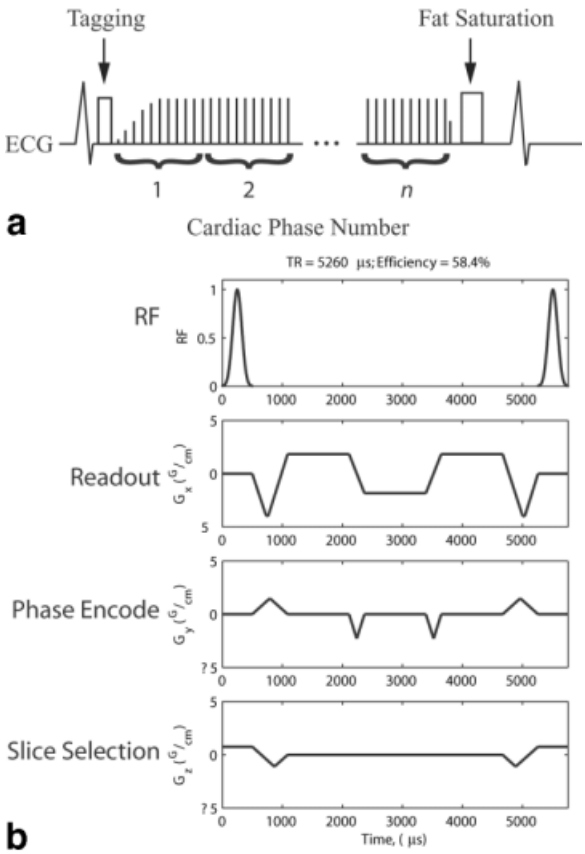


FIG. 1. (**a**) Acquisition schematic: Upon detection of the ECG trigger, the myocardial tagging sequence and a magnetization-restoring sequence were played. Ten TRs were acquired for each cardiac phase using the pulse sequence shown in (**b**), yielding 30 lines of *k*-space per cardiac phase before TSENSE processing. At the end of the imaging period, typically covering 85–95% of the cardiac cycle, a magnetization-storing $\alpha/2$ pulse followed by a fat saturation sequence was applied. (b) displays the three-echo EPI-SSFP sequence used for the single-heartbeat cine acquisitions. The use of gradient optimized waveforms results in the shortest possible TRs and highest efficiency allowed by a given slew rate.

## METHODS

All images were acquired on a 1.5 T CV/i GE scanner (Waukesha, WI, USA) with 40 $mT \cdot m^{-1}$ maximum gradient amplitudes and 180 $T \cdot m^{-1} \cdot s^{-1}$ maximum gradient slew rates. Images were acquired using an eight-channel cardiac phased array coil (Nova Medical, Wilmington, MA, USA) and a locally built eight-channel receiver. All reconstructions were done offline in MATLAB (Natick, MA, USA). Five normal human volunteers were scanned (three male, 31 ± 5 years old, weight 66 ± 15 kg) with full consent and under a protocol approved by the NHLBI institutional review board.

### Imaging Pulse Sequence

The single heartbeat EPI-SSFP sequence was implemented as a three-echo fully balanced sequence, described by Herzka et al. (28). The sequence shown in Fig. 1 takes advantage of the high SNRs and excellent efficiency available with balanced SSFP (13,14). The sequence was optimized using gradient hardware optimized trapezoidal waveforms (21,22) yielding the shortest possible TRs and highest efficiency allowed by the physical gradient amplitudes and slew rates for a Cartesian top-down interleaved trajectory. Due to precise pulse sequence control of the imaging gradients, it was not necessary to apply additional corrections for the use of EPI during image reconstruction although artifacts due to off-resonance spins (i.e., fat) were expected.

Upon detection of the cardiac trigger, the tagging sequence was applied, followed by a magnetization-catalyzing sequence based on the work of Hennig et al. (29),

$$\alpha(n) = \frac{\alpha}{2N} \cdot (2n + 1) \qquad \text{for } 0 \leq n < N$$

$$\alpha(n) = \alpha \qquad \text{for } n \geq N, \qquad [1]$$

where $\alpha$ is the imaging flip angle, $n$ is the RF excitation index, and $N$ is the number of RF pulses to be used in the magnetization restoration pulse sequence (Fig. 1a). Imaging began immediately after tagging, albeit with an expected minor loss in SNR during the first cardiac phase due to the nature of the magnetization restoring sequence, which linearly increases the angle subtended between the magnetization and the *z*-axis over the first $N$ TRs. In this work, typically $N = 5$ was used.

Ten TRs or 30 lines of *k*-space were acquired for each image with temporal resolutions, matrix sizes, and spatial resolutions specified in Table 1. Since field of view (FOV) varied with volunteer, and TR varied with FOV and slice obliquity, all values reported in Table 1 include mean and SD as well as range. After imaging was completed for a given cardiac cycle, a magnetization storing $\alpha/2$ at TR/2 prep pulse and a fat saturation sequence were applied to avoid artifacts from the interruption of steady state at the beginning of the next cardiac cycle. A total of 85–95% of the cardiac cycle was imaged. After the first few cardiac phases, the fat signal returned to its steady-state value although it did not compromise tagged image processing. Typical imaging parameters were as follows: TE = TR/2 for the middle echo, which sampled the central region of *k*-space; $\alpha = 40°$ or 45°; ±125 kHz receiver bandwidth; and 8 mm slice thickness, 75–80% rectangular FOVs ranging from 30 × 22 to 37 × 28 cm. For stripe and grid tagged acquisitions, a symmetric set of five RF pulses with relative weights 0.64, 0.89, and 1.00 were used along with seven pixel tag separation. Acquisitions typically spanned 30–60 consecutive heartbeats. As shown in Table 1 four different readout resolutions of 128, 160, 192, and 256 points and two different $k_y$ resolutions of 90 and 120 lines were acquired for acceleration rates of 3 and 4, respectively.

### Parallel Imaging and Nonaccelerated ($R = 1$) Reconstructions

The TSENSE parallel imaging technique was used to accelerate the acquisition of the single-heartbeat cine loops (24). The last 12 cardiac phases of each cardiac cycle were used to generate a low temporal resolution reference image from which $B_1$ field maps and the coil-dependent sensitivity coefficients were generated. Since the sensitivity coefficients were determined from the original data spanning only a single cardiac cycle, no problems with respect to registration or respiratory motion were encountered and it was unnecessary to perform any other reference scan. Acceleration rates ($R$) of 3 and 4 were used and all images were reconstructed offline using MATLAB (Natick, MA, USA). For $R = 3$ acquisitions 90 $k_y$-line matrix reconstructions were performed while for $R = 4$ 120 $k_y$-line matrix reconstruction was performed, yielding similar temporal resolutions. Note, however, that each line of *k*-space acquired contributed only to a single cardiac phase and no view sharing was utilized: quoted frame rates reflect true temporal resolution. An SNR loss due to the use of parallel imaging can be expected as given by the equation

$$\mathrm{SNR}_{\mathrm{TSENSE}} = \frac{\mathrm{SNR}_{\mathrm{Full}}}{g\sqrt{R}},$$

where $\mathrm{SNR}_{\mathrm{TSENSE}}$ and $\mathrm{SNR}_{\mathrm{Full}}$ are the SNRs obtained using TSENSE and with nonaccelerated, full acquisitions, respectively, $g$ is the loss associated with geometric factors, and $R$ is the acceleration rate used in imaging.

As proposed by the TSENSE method, the lines of *k*-space acquired are varied for successive cardiac phases, leading to an interleaved phase encode ordering. Data from any $R$ contiguous cardiac phases can be combined into a nonaccelerated image with reduced temporal resolution. In a manner analogous to conventional segmented *k*-space imaging, the acquisition line ordering of single heartbeat scans was also interleaved by heartbeat such that the *n*th cardiac phase of any $R$ temporally contiguous heartbeats can be combined and reconstructed into an image. These datasets will be referred to as the nonaccelerated $R$-heartbeat acquisitions and allowed for the reconstruction of datasets that demonstrate the necessity of the single-heartbeat approach.

### Measurement of Myocardial Function

Tag tracking was performed using the FastTag (v 12.2) software, based on the UNTETHER algorithm (30). Motion analysis, including strain calculations, was performed using the methods of Ozturk and McVeigh, based on *B*-spline fitting of the motion fields (31). Typically sets of 25–30 heartbeats were processed. Also, end-systolic (ES) and end-diastolic (ED) LV areas in square millimeters were measured for each heartbeat by manual contouring. Special attention was paid to avoid papillary muscle when contouring. Due to the manually intensive nature of tagged image processing as used in this work, only one of the volunteer's datasets was processed to completion, although images from all volunteers displayed similar conformational changes during Valsalva maneuvers.

### Induction of Transient Myocardial Motion Patterns

To generate a condition during which cardiac function changed visibly in a transient manner from heartbeat to heartbeat, some volunteers were instructed to perform a Valsalva maneuver (32). After breath-holding for 5–10 heartbeats, the subjects undertook extensive expiratory efforts against a closed glottis, similar to the effects observed during coughing and heavy lifting (32). In general, the maneuver greatly increases intrathoracic pressure, causing the collapse of the large veins, impeding venous return, and reducing stroke volume and cardiac output (33). The heart rate increases while blood pressure drops, reducing ventricular volumes. Upon release, a very fast transient drop in arterial pressure is experienced as blood begins to enter the pulmonary vascular bed. Soon thereafter, blood flow and cardiac output return to normal, but not before a small overshoot takes place (33). The maneuver results in highly variable ventricular volumes—particularly for the lower pressure right ventricular cavity—which would lead to artifacts in segmented imaging. Myocardial strains and relative ventricular areas at end-systole and end-diastole during the Valsalva maneuver were calculated and reported. The overall fractional reduction in area, as calculated from the difference of the average of the area measured from the first five breathhold beats and the last five beats during the Valsalva maneuver were reported.

## RESULTS

Figure 2 displays two complete cardiac cycles acquired with the single heartbeat tagging sequence. Figure 2a displays a cine acquired with 192 × 90 matrix using $R = 3$ acceleration, yielding 21 cardiac phases per heartbeat with a temporal

TABLE 1
Typical Temporal Resolutions and Frame Rates Achieved at Various Readout Resolutions

| Readout resolution (points) | Temporal resolution per cardiac phase (ms, mean ± std) (min-max) | Efficiency (η) (%) | Images per second @ 60 BPM | Average spatial resolution | |
|---|---|---|---|---|---|
| | | | | *X*-res (mm) (min-max) | *Y*-res (mm) (min-max) |
| 128 | 34.7 ± 0.6 (33.7–35.6) | 44 | 26 | 2.65 ± 0.21 (2.34–2.89) | $R = 3$ |
| 160 | 39.0 ± 0.9 (37.8–40.5) | 49 | 23 | 2.12 ± 0.17 (1.88–2.31) | 2.88 ± 0.21 (2.50–3.08) |
| 192 | 43.4 ± 1.2 (42.0–45.7) | 53 | 21 | 1.77 ± 0.14 (1.56–1.93) | $R = 4$ |
| 256 | 52.0 ± 1.3 (50.2–54.4) | 59 | 17 | 1.32 ± 0.11 (1.17–1.45) | 2.08 ± 0.19 (1.88–2.25) |

*Note.* Actual TRs are orientation and FOV size dependent and therefore temporal resolution as well as spatial resolution is reported as mean ± standard deviation and (minimum and maximum) values over all volunteers scanned. Average FOV was 33.4 ± 2.8 cm (30–37 cm range). Efficiency, defined as the percentage of time of TR spent acquiring data, was very high for this imaging technique. The number of images per second assumes a 60-beat-per-minute heart rate with imaging over 90% of the cardiac cycle (i.e., 900 ms). The $R = 3$ and $R = 4$ *Y*-resolutions are independent of the *X*-resolution and added in column form due to space concerns.

resolution of 42 ms and spatial resolution of 1.89 × 3.0 mm. The heartbeat displayed is part of an acquisition of 50 consecutive heartbeats. Figure 2b displays a cine acquired with a 256 × 120 matrix using $R = 4$ acceleration, yielding 18 cardiac phases with a temporal resolution of 51 ms and spatial resolution of 1.4 × 2.25 mm. Due to the choice of imaging, flip angle (45°) tags persist in both these acquisitions past early diastole and into diastasis. The use of a flip

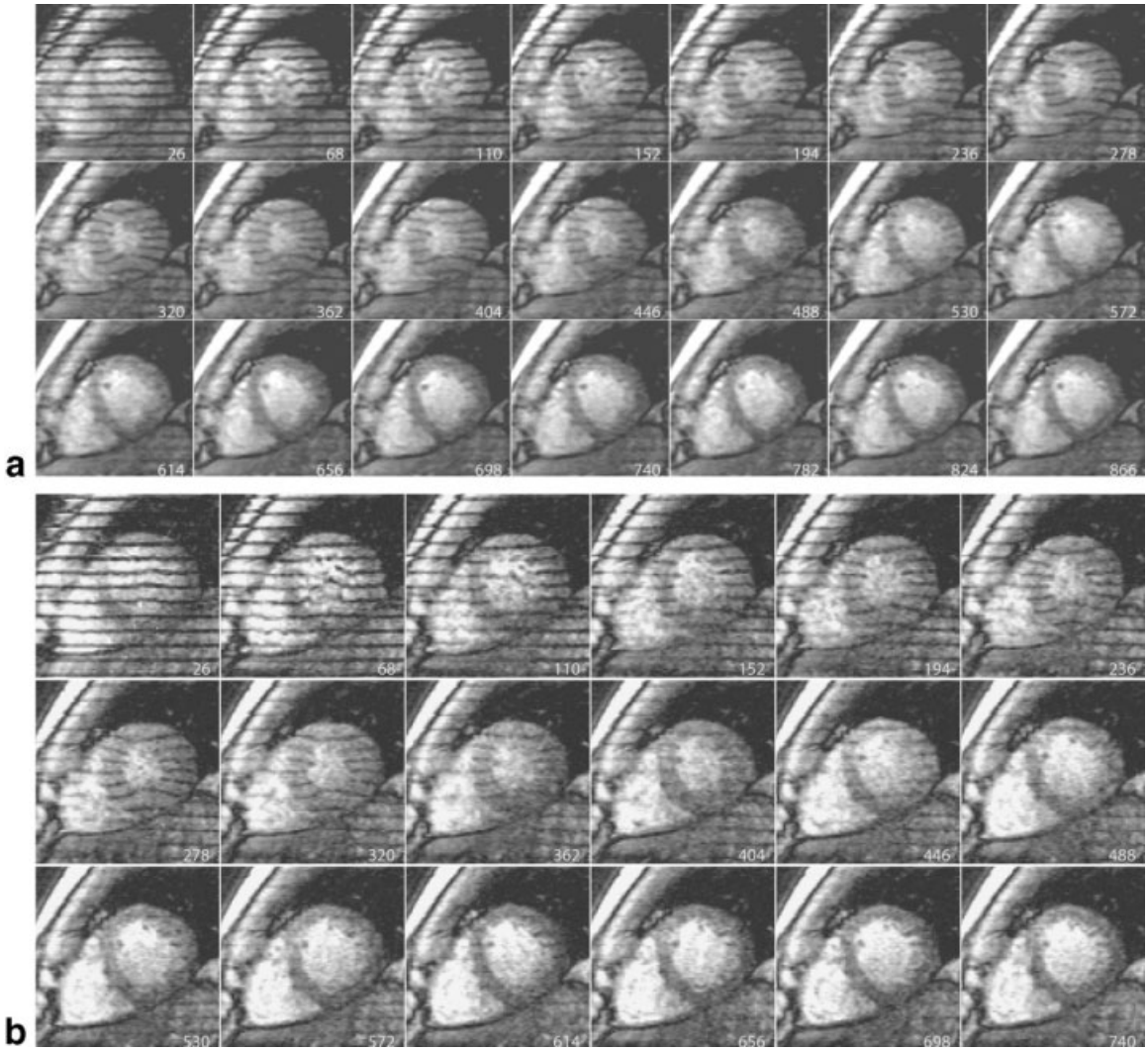


FIG. 2. (**a**) Complete set of single heart beat tagged cine images obtained using $R = 3$ and a 192 × 90 image matrix compose of 21 cardiac phases with a temporal resolution of 42 ms. Tags are clearly visible for all of systole and part of diastole although they disappear by diastasis. Numbers denote time (in milliseconds) after the QRS trigger is detected. (**b**) Example of single heartbeat tagged cine images obtained with $R = 4$ and a 256 × 120 matrix. Eighteen cardiac phases were acquired with a temporal resolution of 51 ms.

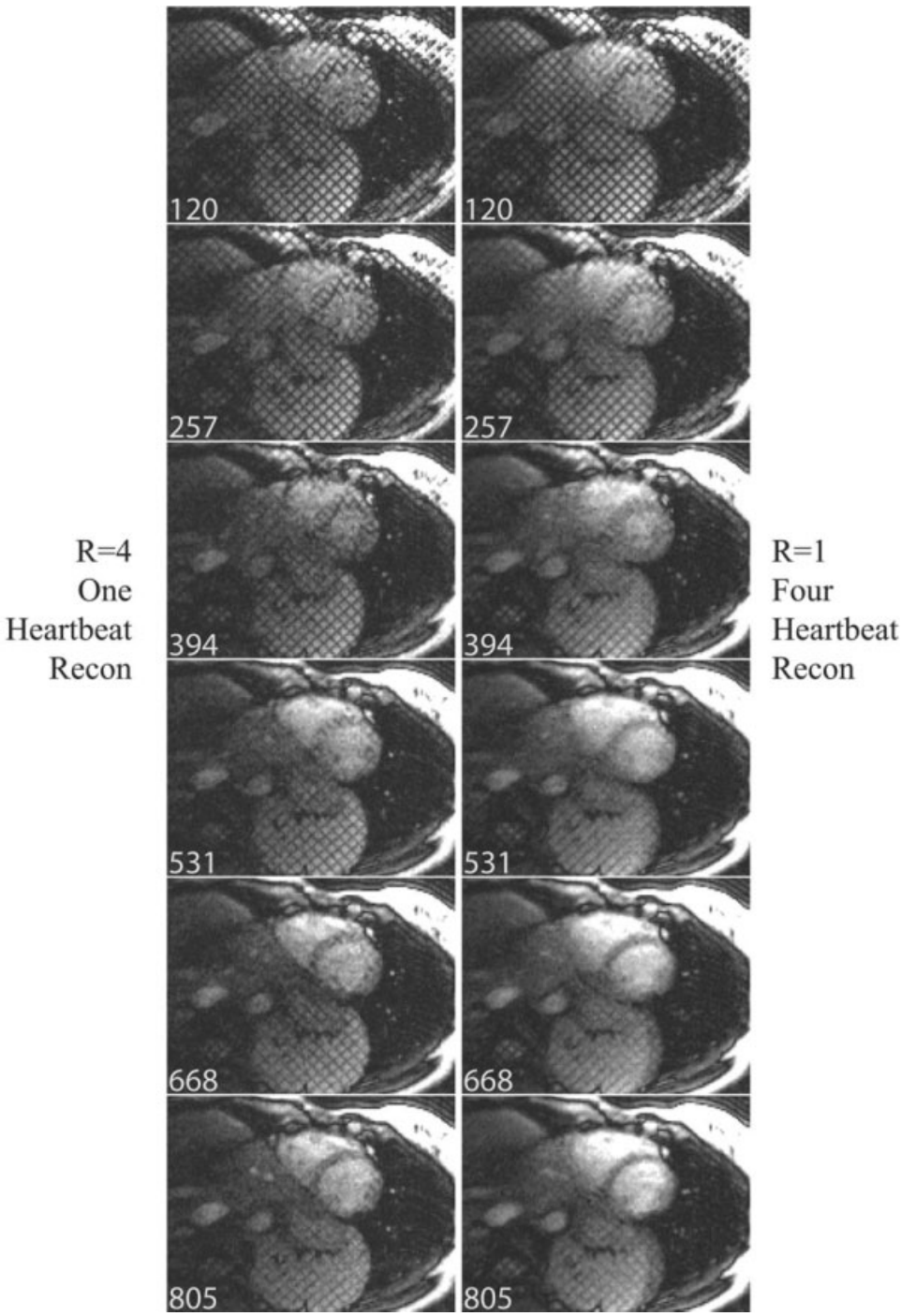


FIG. 3. Comparison of accelerated ($R = 4$, left column) single heartbeat image reconstruction and 4-heartbeat ($R = 1$, right column) reconstruction of the same raw data acquired during breathing. Tag blurring is obvious both in the heart and in other moving organs such as the liver for the standard nonaccelerated reconstruction. Note that the blurring also affects tag visibility in the later cardiac phases. Numbers denote time in milliseconds after ECG trigger. Images window/leveled differently: (38/15 versus 120/49).

angle ramp allows for complete visualization of the tags in the first cardiac phase.

Figure 3 displays a comparison of exactly the same raw data acquired during regular breathing reconstructed in two different manners. The left column displays single heartbeat data reconstructed using TSENSE ($R = 4$), while the right column displays the equivalent data reconstructed without parallel imaging ($R = 1$). Note that the tags persist longer on the accelerated images compared to the corresponding ones reconstructed from multiple heartbeats due to the elimination of blurring due to interheartbeat motion. This is particularly obvious in the liver, which moves drastically during breathing.

Figure 4 displays the end-diastolic cardiac phase (21st of 21) for 25 heartbeats acquired during a Valsalva maneuver. LV cavity contours are displayed for easy assessment of conformation changes. The acquisition was done with a $192 \times 90$ matrix, $R = 3$, and $36 \times 27$ cm FOV and achieved a temporal resolution of 42 ms and a spatial resolution of $1.8 \times 3.0$ mm. The volunteer was asked to breath-hold for the first 5 heartbeats. The effect of the maneuver becomes apparent by the 8th heartbeat as evidenced by the flattening of the inferior wall. The increased pressure was maintained until the 21st heartbeat, after which the volunteer breathed heavily. Due to the rapid changes in heart rate, some ECG triggers were missed during the onset of breath-

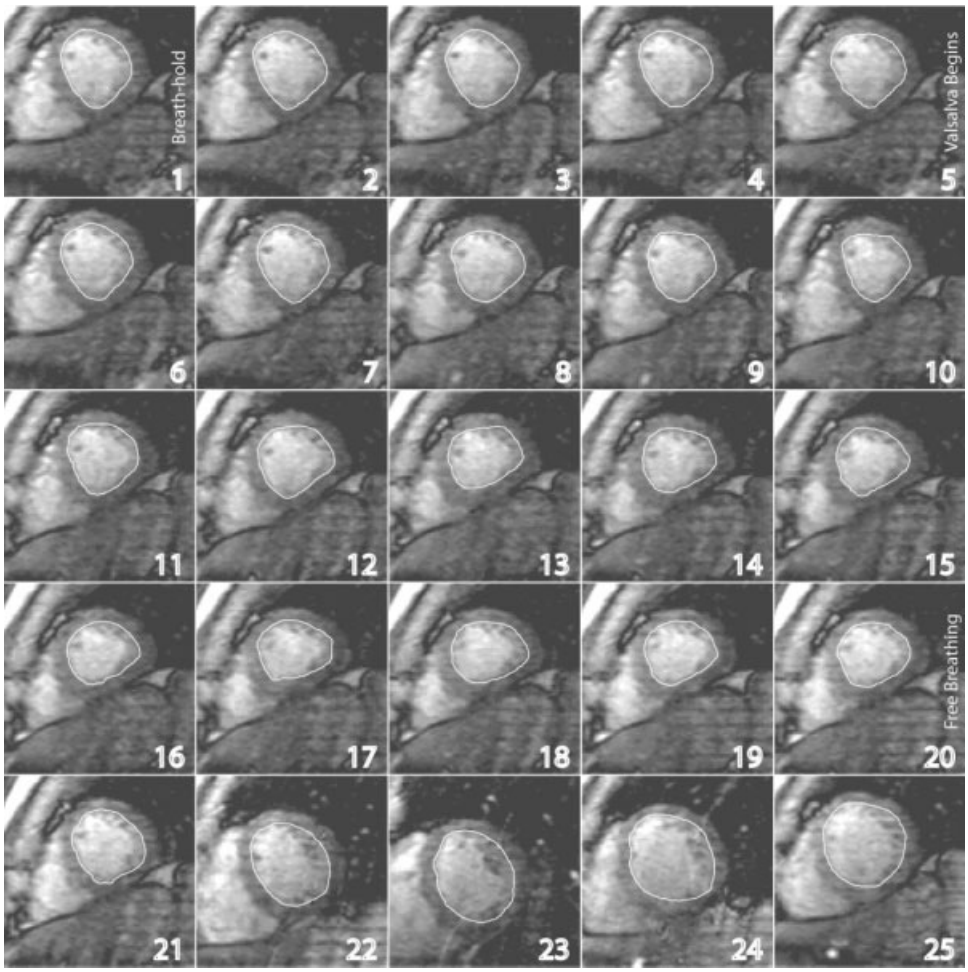


FIG. 4. The end-diastolic cardiac phase for a 25-heartbeat acquisition during a Valsalva maneuver. LV chamber contours are displayed in white and heartbeat number is displayed in the bottom right-hand corner of each image. The effects of the Valsalva maneuver are evident in the diastolic images, where the heart's conformational change is obvious. After breath-holding for 5 heartbeats, the maneuver begins reducing the size of both the LV and the RV. When viewed in movie mode, the flattening of the posterior wall becomes obvious. The increased intrathoracic pressure persists until the 21st heartbeat, when breathing resumes. The data from each heartbeat consisted of 21 cardiac phases with a temporal resolution of 42 ms and a 192 $\times$ 120 matrix acquired over a 36 $\times$ 27 cm FOV.

ing after the maneuver, causing the omission of the immediately following cardiac cycles. Through-plane motion is also apparent in the images from the last 4 heartbeats. Conformational changes due to the increased intrathoracic pressure are readily observed with the LV contours. Note that were these data, or a subset thereof, used for generation of images with the standard segmented imaging methods, artifacts and blurring would result.

The results of the strain analysis performed on the series of beats showcased in Fig. 4 are displayed in Fig. 5. Data displayed are for two of six radial segments of myocardium, the lateral (left) and septal (right) walls. The *y*-axis (vertical) corresponds to cardiac phase while the *x*-axis (horizontal) corresponds to heartbeat number. As expected, there is very little difference between the strain patterns observed during the first five beats of the acquisition due to the nature of breath-holding. However, the data acquired during the Valsalva maneuver display changes in the strain patterns, particularly on the lateral wall. Also, strain patterns are even more distinct once free breathing resumes (~beat 21) although through-plane motion was apparent (Fig. 4).

Figure 6 displays the relative end-systolic right ventricular area (a), left ventricular end systolic (b), and end-diastolic (c) areas as measured by contouring from the dataset in Fig. 4. Area values of the last five heartbeats were excluded due to obvious through-plane motion. Note how the right ventricular area drops at the onset of the maneuver (beat 5) although it takes a few beats for the drop in venous return to propagate to the left ventricular cavity.

## DISCUSSION

### Imaging Technique

The presented technique produced cine images from a single cardiac cycle, removing the temporal averaging over multiple heartbeats found in segmented imaging. Image quality was maintained under conditions that displayed beat-to-beat variations and would produce artifacts in acquisitions spanning several heartbeats. Furthermore, the technique achieved high spatial and temporal resolutions in a real-time imaging setting, as shown in Table 1. For the

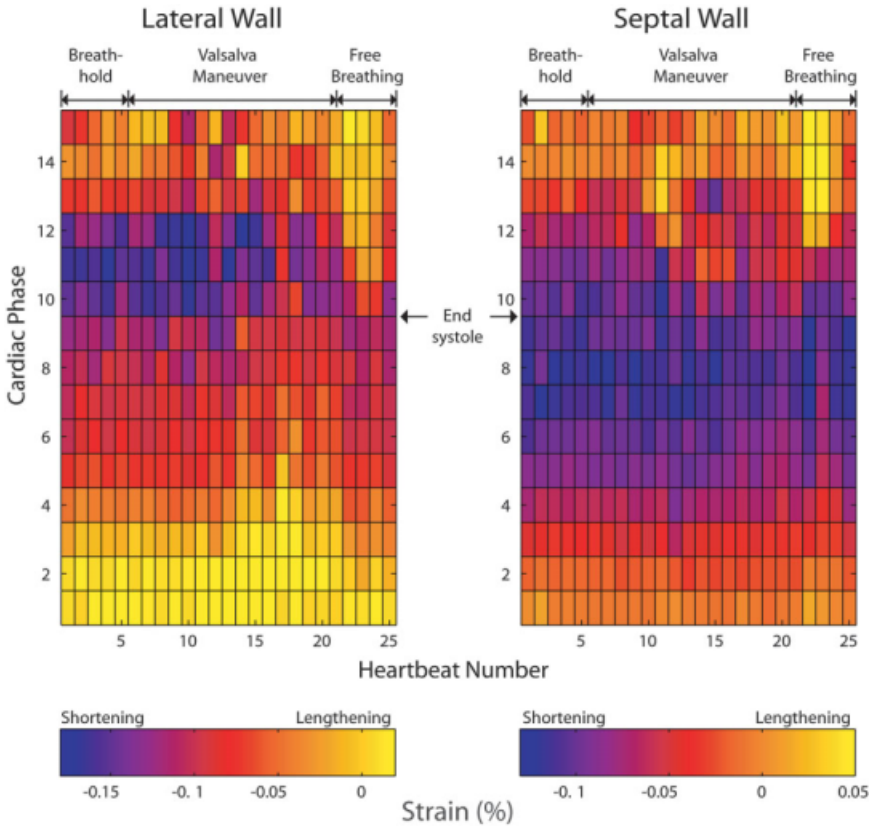


FIG. 5. Strains (% fractional shortening) along the tag direction in lateral (left) and septal (right) segments derived from the images showcased in Fig. 4. The vertical axes correspond to cardiac phase for each heartbeat; the horizontal axes denote heartbeat number creating a temporal plane that progresses from bottom to top and from left to right. Although the maneuver begins after the 5th heartbeat, strains do not appreciably change until later heartbeats. Breathing resumes during the 21st beat, again changing strain patterns. Note that beat 12 displays a different strain pattern than other neighboring beats, indicating beat-to-beat differences that would lead to image artifact in a segmented acquisition. These patterns are seen as changes in conformation when viewed in cine mode.

typical FOV of 36 × 27 cm used with volunteers in this work, imaging with a 192 × 90 ($R = 3$) matrix achieved a temporal resolution of 42 ms and a spatial resolution of 1.88 × 3.00 mm. Similarly, for a matrix size of 256 × 20, a temporal resolution of 51 ms was achieved with a spatial resolution of 1.41 × 2.25 mm. This combination of spatial and temporal resolutions has not been demonstrated before in "real-time" cardiac imaging, primarily because of the focus on low latency reconstruction that is not implemented in this work.

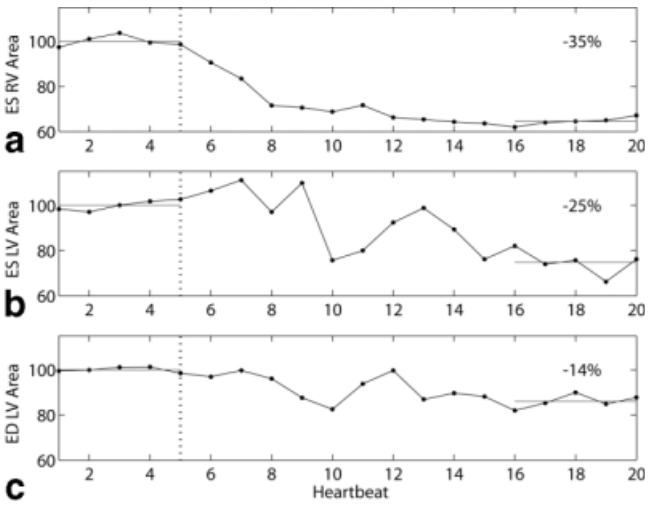


FIG. 6. Plots of relative (**a**) end-systolic right ventricular area, (**b**) end-systolic left ventricular area, and (**c**) end-diastolic left ventricular area measured over the initial 20 heartbeats displayed in Fig. 4. Upon initiation of the Valsalva maneuver (beat 5, dotted line), the right ventricular volume decreases, and after 2–3 beats the left ventricular volumes follow. Overall, the right ventricle (a low pressure cavity) decreases much more than either of the left-ventricular volumes.

Previous measures of cardiac function using real-time images were limited in terms of spatial or temporal resolution. Other work relied on gradient echo imaging together with EPI readouts with long echo trains (7–14 readouts). Here, the use of SSFP provides higher SNR than the gradient echo acquisitions used typically used with EPI (28). Furthermore, the use of EPI with long readouts in cardiac imaging can have detrimental effects on image quality due to image distortion form field inhomogeneity, short $T_2$*, and multiple phase discontinuities (9,11). Here, a short three-echo readout is used and the interecho spacing is minimized by the use of hardware optimized trapezoidal gradient waveforms, reducing distortion from both sources. Furthermore, the three-echo sequence generates echoes that refocus field inhomogoneities as the center of *k*-space is sampled (34). And although no correction is applied for off-resonant spins (i.e., echo-time shifting (11), image quality was adequate for accurate measurement of regional function (see Fig. 2).

## Parallel Imaging

High acceleration rate parallel imaging (with offline reconstruction) was applied to every acquisition, at the cost of SNR loss due to geometric factors. As expected, the use of

$R = 3$ generally had better image quality although at lower resolutions in the phase encode direction than the $R = 4$ acquisitions (90 versus 120 $k_y$-lines). While $R = 4$ acquisitions were used to increase spatial resolution, these acquisitions could have had improved temporal resolution, particularly when acquiring 256 readout points. For example, a $256 \times 96$ matrix would have had a temporal resolution of ~42 ms, yielding the same temporal resolution as the typical $192 \times 120$ scans. Similarly, a $192 \times 96$ $R = 4$ reconstruction would have had a temporal resolution of ~34 ms—the same resolution as the $128 \times 120$ scans. This trade-off could be beneficial for stripe tagged acquisitions, were most of the relevant information about motion is located in the lower frequency $k_y$-lines.

The use of high acceleration rates is not common in 2D imaging due to the price paid in SNR efficiency. The larger *g*-factor losses may severely compromise image quality, although this problem will be ameliorated with the upcoming release of 16- and 32-receiver channel systems. The larger number of coils will allow for more stable and better conditioned reconstruction of undersampled data as well as increased SNR. Furthermore, as optimized algorithms for reconstruction are implemented on faster processors and on a larger number of processors, higher acceleration reconstructions will be possible in true real-time fashion: little to no latency between acquisition and display. In the current work, offline reconstruction took approximately 10–20 s per heartbeat, depending on the matrix size. However, reconstruction was not optimized for speed and implemented in a generally slow platform (MATLAB).

For validation of the single heartbeat tagging technique, the raw data were also reconstructed without TSENSE acceleration, that is, by combining four contiguous heartbeats in a sliding window manner. This type of reconstruction was possible as phase encode acquisitions were not only interleaved by cardiac phase, as suggested by the TSENSE method, but also by heartbeat. These nonaccelerated cine loops ($R = 1$) displayed higher SNR at the expense of blurring and tag persistence. This is particularly obvious in Fig. 3, where tags persist for longer in the accelerated ($R = 4$) images and the edges of structures are less blurred (e.g., the liver's movement from breathing). Note that two different $R = 2$ reconstructions could also have been possible with the same datasets, although none are displayed here: a contiguous paired two-heartbeat and a contiguous paired two-cardiac phase reconstruction (e.g., beats 1 and 2, beats 3 and 4, and Phases 1 and 2, Phases 3 and 4).

In the context of general cardiac imaging where the majority of successive heartbeats are expected to be substantially similar to one another, the heartbeat-interleaved acquisition could be used for selective combining of beats for SNR gain (35). In this scenario, the single heartbeat parallel-reconstructed images would act as a self-navigator used to determine candidates for combination, providing a Cartesian sampling equivalent of projection reconstruction self-gated techniques (36) or variable density spiral imaging (37). The images reconstructed with high acceleration rates can be used to determine whether the current heartbeat is acceptable in terms of respiratory phase or other motion, yielding a non-breath-held, high SNR cine loop from the multiheartbeat dataset. Furthermore, because the present technique uses data matrices with high spatial resolutions and generates images with high temporal resolutions, the resulting averaged acquisitions would be of similar quality to standard cine acquisitions in terms of resolution.

### Measurement of Myocardial Function Using Tagging

Images were acquired during a Valsalva maneuver, as a demonstration of the single heartbeat tagging technique in use during rapid, beat-to-beat changes in cardiac function. Figure 4 displays diastolic images while Fig. 6 displays the area curves for the first 20 heartbeats obtained from the results of a single normal volunteer. Looking at the right ventricular areas in Fig. 6a, it can be seen that the right ventricle begins to reduce in size immediately upon the initiation of the Valsalva maneuver. This is expected, as the large increase in intrathoracic pressure as well as the collapsing of the large veins and reduction of venous return are all bound to reduce the RV volume. The right ventricular area decreased by 35%, which compares favorably with the results from Little et al. (38), who saw a decrease of ~40% in ED RV area using echocardiography. The ED and ES left ventricular areas decreased 15 and 25%, respectively, as shown in Fig. 6. These results are similar the previously published results from Robertson et al. (39), who saw decreases of 11.2 and 9.5% for the ED and ES dimension from 1D echocardigraphy. Adjusting the results from Robertson et al. for the differences between 1D and 2D measurements and assuming a circular ventricle, 1D decreases in dimension of 11.2 and 9.5% are equivalent to 21 and 18% decreases in area. These results are therefore consistent with those obtained with single heartbeat MR imaging.

The single heartbeat tagging technique has also demonstrated changes in strain patterns during the maneuver (Fig. 5). It is important to point out that the strain patterns obtained from the first 5 breath-held heartbeats are very similar, indicating that the single heartbeat tagging technique is stable. Also, the strain patterns of the first few beats within the Valsalva maneuver are not very distinct from those of the first 5 beats. This can be explained by the fact that the right-ventricular pressure drop takes a few heartbeats to propagate fully to the left ventricular system. Robertson et al. (39) report that the minimum LV dimension is not reached until 12–20 beats after initiation of the maneuver. Similarly, Nishimura et al. (33) also demonstrate data where the decreases in arterial blood pressure do not begin until the 10th beat of the Valsalva maneuver. In fact, the strain patterns displayed by beats 10–15 beats after initiation of the maneuver do display changing strain patterns. For example, there is a delay in the onset of systole from heartbeats 14 to 20 in the lateral wall (Fig. 5, left, bottom). It is important to realize that strains are computed relative to the first cardiac phase of each individual heartbeat. In general, if measurements were made relative to the configuration of the first cardiac phase of the initial non-Valsalva heartbeat, greater differences in strain patterns could be observed. From Fig. 4 it is obvious that the end diastolic relaxed state of the myocardium has become stretched during the Valsalva maneuver; it is an interesting observation that the dynamic range of the strain

is so remarkably preserved. In any case, the variable nature of the acquisition highlights the need for a technique that can measure regional function heartbeat to heartbeat.

### Technique Limitations

Single, 2D slice imaging of motion as used in this work has limitations with respect to through-plane motion. Specifically, the slice position is not adjusted to follow the material (i.e., slice following), so a different material location may be imaged for each cardiac phase. This is a problem common to many well-established cardiac imaging techniques. Unfortunately, most slice tracking methods are based on subtraction techniques, requiring multiple heartbeat acquisitions, and thus could not be utilized in their present form for this work.

The impact of uncompensated through-plane motion is dependent on several factors including the net displacement in the through-plane direction and the changes in geometry and heterogeneity of the underlying object being imaged. In this work, a mid-level short axis slice was chosen: such a slice is expected to have a maximum displacement less than approximately one slice width (~10 mm). For this prescription, and for acquisitions without severe respiratory motion, the geometry of the heart is relatively uniform in the through-plane direction, minimizing the changes induced by through-plane motion on the strain data. Also, for this type of experiment, and for the proposed research experiments (next section), physiologic changes are assumed to affect the heart as a whole, implying that the response of the myocardium to the transient conditions, e.g., the Valsalva maneuver, will produce strain values that vary slowly in the long axis direction.

One focus of this work is to demonstrate strain measurements and observe variations in strain between corresponding cardiac phases from heartbeat to heartbeat. In terms of Fig. 5, the most important new information is found in the variation along the horizontal axis. Even if through-plane motion does have an effect on each individual cardiac phase within a cardiac cycle, approximately that same motion would affect subsequent cardiac cycles too, and so heartbeat-to-heartbeat variations, i.e., the data of interest, would be preserved. For example, Fig. 4 presents a sequence of images of a single diastolic cardiac phase for multiple heartbeats throughout a Valsalva maneuver. There is little change in the appearance of the slice being imaged from heartbeat to heartbeat. Although this does not discount through-plane motion, it implies that any through-plane motion is causing minimal changes in the measured strains. In image 23, there is a clear change in conformation introduced by the resumption of breathing in a severe and abrupt manner. In fact, once breathing resumes, through-plane motion greatly increases and no valid comparisons can be made with previous data. The same can be said of Fig. 5, where strain data are presented. Looking at strain in the lateral wall, it is possible to see that strains change radically once breathing is resumed. These changes could be due to the resumption of blood flow or from through-plane motion, but given the limited nature of single slice imaging, it is not possible to determine conclusively.

The effects of through-plane motion probably do not have a major effect on the strain results presented here. It is important to note that, if imaging under conditions where there is larger variability in the myocardium in the long-axis dimension, through-plane motion will have larger effects on the measures of regional function. For example, if looking at a small infarct model with significant heterogeneity in the long-axis dimension, measures of strains as presented here could be compromised.

### Imaging Applications

The presented technique, in its current implementation, is designed as a tool for the study of cardiac function. One application where the combination of high spatial and temporal resolutions may be of use is the generation of rapid ventricular volume and ejection fraction measurements concurrent with regional function. As suggested by Nayak and Hu (8) and Bornsted et al. (5), one slice could be imaged per heartbeat, obtaining complete heart coverage within one breath-hold. Furthermore, such an acquisition could easily include both long and short axis slices, allowing for true 3D measurement of strains (30,31). Other applications could include stress testing (3), although use of matrix sizes that yield higher temporal resolutions (i.e., $192 \times 96$, $R = 4$) might be necessary due to the increased heart rate (2). Furthermore, visual examination of tags can qualitatively point to cardiac dysfunction earlier in the exam if a low latency reconstruction were applied. Single heartbeat imaging might also be able to correctly image transient wall motion patterns developed during the stress test that the conventional 10-heartbeat segmented imaging sequence might mask due to temporal averaging.

The use of single heartbeat myocardial tagging can also be used for the determination of single heartbeat fiber stress–fiber length loops analogous to the pressure–volume loops used for analysis of cardiac mechanics and as described by Prinzen et al. (40) for segmented acquisitions. Such application could yield another tool for the study of cardiac function and contractility during changes in pacing rate, pacing location or from changes in preload, and afterload, all of which can result in drastic changes in global function from state to state. Similarly, the technique could be used for the study of premature ventricular contractions or ectopic beats, both of which are currently not being studied with MRI.

Finally, combined with a low latency reconstruction, the single heartbeat tagging technique could find multiple uses within the field of interventional MRI. For example, ethanol injections and RF ablations are used as treatments for cardiomyopathies and rhythm disorders and direct visualization of tag motion could provide immediate feedback on the extent and success of treatment.

## CONCLUSION

We have presented a fast imaging technique for the measurement of regional cardiac function within a single heartbeat, which allows for the monitoring of function during transient cardiac events. The technique combined the use of a high-efficiency, gradient-optimized EPI-SSFP sequence with high acceleration factor parallel imaging and achieved a combination of high spatial and temporal resolutions. Measurement of cardiac function through

transient phenomena was demonstrated with the use of Valsalva maneuvers, during which intrathoracic pressure caused distinct changes in function in a beat-to-beat nature. A comparison with nonaccelerated reconstruction of the same raw data confirmed the benefits of single heartbeat imaging by reducing both motion artifacts and tag blurring.

## ACKNOWLEDGMENTS

The authors thank Dr. H. D. Morris for the help with the development of the 8-channel receiver array and Dr. D. B. Ennis for his help on strain analysis and processing. Also we thank Dr. T. S. Denney, Jr. for the use of his FastTag software.

## REFERENCES

1. Chapman B, Turner R, Ordidge RJ, Doyle M, Cawley M, Coxon R, Glover P, Mansfield P. Real-time movie imaging from a single cardiac cycle by NMR. Magn Reson Med 1987;5:246–254.
2. Setser RM, Fischer SE, Lorenz CH. Quantification of left ventricular function with magnetic resonance images acquired in real time. J Magn Reson Imaging 2000,12:430–438.
3. Schalla S, Klein C, Paetsch I, Lehmkuhl H, Bornstedt A, Schnackenburg B, Fleck E, Nagel E. Real-time MR image acquisition during high-dose dobutamine hydrochloride stress for detecting left ventricular wall-motion abnormalities in patients with coronary arterial disease. Radiology 2002;224:845–851.
4. Nagel E, Schneider U, Schalla S, Ibrahim T, Schnackenburg B, Bornstedt A, Klein C, Lehmkuhl HB, Fleck E. Magnetic resonance real-time imaging for the evaluation of left ventricular function. J Cardiovasc Magn Reson 2000;2:7–14.
5. Bornstedt A, Nagel E, Schalla S, Schnackenburg B, Klein C, Fleck E. Multi-slice dynamic imaging: complete functional cardiac MR examination within 15 seconds. J Magn Reson Imaging 2001;14:300–305.
6. Lee VS, Resnick D, Bundy JM, Simonetti OP, Lee P, Weinreb JC. Cardiac function: MR evaluation in one breath hold with real-time true fast imaging with steady-state precession. Radiology 2002;222:835–842.
7. Shankaranarayanan A, Simonetti OP, Laub G, Lewin JS, Duerk JL. Segmented k-space and real-time cardiac cine MR imaging with radial trajectories. Radiology 2001;221:827–836.
8. Nayak KS, Hu BS. Triggered real-time MRI and cardiac applications. Magn Reson Med 2003;49:188–192.
9. Reeder SB, Faranesh AZ, Boxerman JL, McVeigh ER. In vivo measurement of T*2 and field inhomogeneity maps in the human heart at 1.5 T. Magn Reson Med 1998;39:988–998.
10. Reeder SB, Atalar E, Bolster BD, Jr, McVeigh ER. Quantification and reduction of ghosting artifacts in interleaved echo- planar imaging. Magn Reson Med 1997;38:429–439.
11. Feinberg DA, Oshio K. Phase errors in multi-shot echo planar imaging. Magn Reson Med 1994;32:535–539.
12. Duerk JL, Simonetti OP. Theoretical aspects of motion sensitivity and compensation in echo-planar imaging. J Magn Reson Imaging 1991;1:643–650.
13. Oppelt A, Graumann R, Barfub H, Fischer H, Hartl W, Schajor W. FISP—a new fast MRI sequence. Electromedica 1986;54:15–18.
14. Sekihara K. Steady-state magnetization in rapid NMR imaging using small flip angles and short repetition intervals. IEEE Trans Med Imaging 1987;6:157–164.
15. Schaeffter T, Weiss S, Eggers H, Rasche V. Projection reconstruction balanced fast field echo for interactive real-time cardiac imaging. Magn Reson Med 2001;46:1238–1241.
16. Spuentrup E, Schroeder J, Mahnken AH, Schaeffter T, Botnar RM, Kuhl HP, Hanrath P, Gunther RW, Buecker A. Quantitative assessment of left ventricular function with interactive real-time spiral and radial MR imaging. Radiology 2003;227:870–876.
17. Riederer SJ, Tasciyan T, Farzaneh F, Lee JN, Wright RC, Herfkens RJ. MR fluoroscopy: technical feasibility. Magn Reson Med 1988;8:1–15.
18. Wintersperger BJ, Nikolaou K, Dietrich O, Rieber J, Nittka M, Reiser MF, Schoenberg SO. Single breath-hold real-time cine MR imaging: improved temporal resolution using generalized autocalibrating partially parallel acquisition (GRAPPA) algorithm. Eur Radiol 2003;13:1931–1936.
19. Guttman MA, Kellman P, Dick AJ, Lederman RJ, McVeigh ER. Real-time accelerated interactive MRI with adaptive TSENSE and UNFOLD. Magn Reson Med 2003;50:315–21.
20. Weiger M, Pruessmann KP, Boesiger P. Cardiac real-time imaging using SENSE. Sensitivity encoding scheme. Magn Reson Med 2000;43:177–184.
21. Derbyshire JA, McVeigh ER. GROMIT: a SSFP imaging sequence employing hardware optimized gradients and just-in-time waveform synthesis [abstract]. In: Proceedings of the 10th Annual Meeting of ISMRM, Honolulu, 2003. p 2359.
22. Atalar E, McVeigh ER. Minimization of dead-periods in MRI pulse sequences for imaging oblique planes. Magn Reson Med 1994;32:773–777.
23. Herzka DA, Guttman MA, McVeigh ER. Myocardial tagging with SSFP. Magn Reson Med 2003;49:329–340.
24. Kellman P, Epstein FH, McVeigh ER. Adaptive sensitivity encoding incorporating temporal filtering (TSENSE). Magn Reson Med 2001;45:846–852.
25. Axel L, Dougherty L. Heart wall motion: improved method of spatial modulation of magnetization for MR imaging. Radiology 1989;172:349–350.
26. Zerhouni EA, Parish DM, Rogers WJ, Yang A, Shapiro EP. Human heart: tagging with MR imaging–a method for noninvasive assessment of myocardial motion. Radiology 1988;169:59–63.
27. McVeigh ER, Atalar E. Cardiac tagging with breath-hold cine MRI. Magn Reson Med 1992;28:318–327.
28. Herzka DA, Kellman P, Aletras AH, Guttman MA, McVeigh ER. Multishot EPI-SSFP in the heart. Magn Reson Med 2002;47:655–664.
29. Hennig J, Speck O, Scheffler K. Optimization of signal behavior in the transition to driven equilibrium in steady-state free precession sequences. Magn Reson Med 2002;48:801–809.
30. Denney TS Jr, Gerber BL, Yan L. Unsupervised reconstruction of a three-dimensional left ventricular strain from parallel tagged cardiac images. Magn Reson Med 2003;49:743–754.
31. Ozturk C, McVeigh ER. Four-dimensional B-spline based motion analysis of tagged MR images: introduction and in vivo validation. Phys Med Biol 2000;45:1683–1702.
32. Berne RM, Levy MN. Control of cardiac output: coupling of heart and blood vessels. In: Kist K, editor. Cardiovascular physiology. Sixth ed. St. Louis: Mosby–Year Book; 1992. p 194–218.
33. Nishimura RA, Tajik AJ. The Valsalva maneuver and response revisited. Mayo Clin Proc 1986;61:211–217.
34. Scheffler K, Hennig J. Is TrueFISP a gradient-echo or a spin-echo sequence? Magn Reson Med 2003;49:395–397.
35. Hardy CJ, Saranathan M, Zhu Y, Darrow RD. Coronary angiography by real-time MRI with adaptive averaging. Magn Reson Med 2000;44:940–946.
36. Larson AC, White RD, Laub G, McVeigh ER, Li D, Simonetti OP. Self-gated cardiac cine MRI. Magn Reson Med 2004;51:93–102.
37. Sussman MS, Stainsby JA, Robert N, Merchant N, Wright GA. Variable-density adaptive imaging for high-resolution coronary artery MRI. Magn Reson Med 2002;48:753–764.
38. Little WC, Barr WK, Crawford, MH. Altered effect of the Valsalva maneuver on left ventricular volume in patients with cardiomyopathy [abstract]. Circulation 1985;71:227–233.
39. Robertson D, Stevens RM, Friesinger GC, Oates JA. The effect of the Valsalva maneuver on echocardiographic dimensions in man. Circulation 1977;55:596–562r.
40. Prinzen FW, Hunter WC, Wyman BT, McVeigh ER. Mapping of regional myocardial strain and work during ventricular pacing: experimental study using magnetic resonance imaging tagging. J Am Coll Cardiol 1999;33:1735–1742.